J Nanopart Res (2018) 20: 46
https://doi.org/10.1007/s11051-018-4146-1

BRIEF COMMUNICATION

Reduced graphene oxide supported gold nanoparticles for electrocatalytic reduction of carbon dioxide

Mohammad Saquib · Aditi Halder

Received: 31 August 2017 / Accepted: 24 January 2018 / Published online: 19 February 2018

Abstract Electrochemical reduction of carbon dioxide is one of the methods which have the capability to recycle CO_2 into valuable products for energy and industrial applications. This research article describes about a new electrocatalyst "reduced graphene oxide supported gold nanoparticles" for selective electrochemical conversion of carbon dioxide to carbon monoxide. The main aim for conversion of CO_2 to CO lies in the fact that the latter is an important component of syn gas (a mixture of hydrogen and carbon monoxide), which is then converted into liquid fuel via well-known industrial process called Fischer-Tropsch process. In this work, we have synthesized different composites of the gold nanoparticles supported on defective reduced graphene oxide to evaluate the catalytic activity of reduced graphene oxide (RGO)-supported gold nanoparticles and the role of defective RGO support towards the electrochemical reduction of CO_2. Electrochemical and impedance measurements demonstrate that higher concentration of gold nanoparticles on the graphene support led to remarkable decrease in the onset potential of 240 mV and increase in the current density for CO_2 reduction. Lower impedance and Tafel slope values also clearly support our findings for the better performance of RGOAu than bare Au for CO_2 reduction.

Keywords Reduced graphene oxide gold nanoparticles · Carbon dioxide reduction · Onset potential · Impedance spectroscopy · Tafel slope · Energy applications

Introduction

The total usage of fossil fuel comprises ~81.5% of global energy resources which emits carbon dioxide as a byproduct and one of the major components (93%) of the total greenhouse gases by International Energy Agency, 2016 report. The long lifetime of CO_2 in the atmosphere hinders the stabilization of concentration of different greenhouse gases at any level (Middleton and Eccles 2013). It is important to find out an alternative pathway to convert this anthropogenic CO_2 into useful products (Whipple and Kenis 2010; Köleli et al. 2003). To reduce atmospheric CO_2 into useful products has a broader area of research and electrochemical reduction is one of them (Benson et al. 2009; Hori et al. 1987, 1989). Electrochemical reduction of carbon dioxide is a process by which carbon dioxide can be electrochemically reduced to different chemical species. The major challenges are that by electrochemical reduction of carbon dioxide, multiple products are formed with a high overpotential (Hori 2008). An efficient catalyst should control the multi-electron and proton transfer pathways for CO_2 with low overpotential and selective reduction of CO_2 to a particular desired product. So far, only few

Electronic supplementary material The online version of this article (https://doi.org/10.1007/s11051-018-4146-1) contains supplementary material, which is available to authorized users.

M. Saquib · A. Halder (✉)
School of Basic Sciences, Indian Institute of Technology Mandi, Mandi, Himachal Pradesh 175005, India
e-mail: aditi@iitmandi.ac.in

catalysts are available which can selectively give the desired fuel from CO_2. Hence, it is important to develop a catalyst which can overcome the large kinetic barrier of electrochemical reduction of CO_2 (Bradford and Vannice 1999; Nie et al. 2013; Jitaru 2007; Lei et al. 2016) with single end product. In this article, we focused on the study of an electrocatalyst which will selectively reduce CO_2 into CO at lower electrode potential with higher current densities. The reason behind the selective conversion of CO_2 is that CO is an important component of syn gas which is a mixture of hydrogen and carbon monoxide. Syn gas can be then converted into liquid fuel via a well-known industrial process called Fischer-Tropsch process.

In the notable work of Hori (Hori et al. 1985), several metals had been used to study the performance of CO_2 reduction and it was shown how the faradic efficiency and the nature of end product was dependent upon the type of metal catalysts used. Among the various metal catalysts, Cu electrodes preferentially produce hydrocarbons and alcohols whereas Au, Ag, Zn, Pd, and Ga show higher amount of CO production. The highest faradic efficiency for CO_2 reduction to CO was observed on Au electrodes. Au can withstand one of the most critical challenges in the electrochemical conversion of CO_2, i.e., CO_2^- radical stabilization along with high CO selectivity in aqueous as well as in non-aqueous electrolytes. Several work had been reported to establish the fact that gold is one of the best metal for the selective conversion of CO_2 to CO, e.g., the recent work of Sun et al. (Zhu et al. 2013) showed that monodisperse gold nanoparticles selectively reduces CO_2 to CO. Oxide-derived gold nanoparticles could reduce aqueous CO_2 to CO at a very low overpotential (Chen et al. 2012). Detailed literature survey reveals that gold is the best choice for an electrode material among various other materials with highest activity and selectivity for CO_2 reduction to CO (Hori 2008). However, limited study has been carried out to understand the role of support materials on the electrochemical reduction of carbon dioxide by gold catalyst.

Recently, graphene nanosheets drew a great attention towards itself as a good support material because of its high conductivity (10^3–10^4 S/m), large surface area (~ 2600 m^2/g), and low manufacturing costs (Stankovich et al. 2006; Geim and Novoselov 2007; Park and Ruoff 2009). It also showed very promising results for a variety of applications such as methanol oxidations (Li et al. 2009; Dong et al. 2010a), supercapacitors (Liu et al. 2010; Yan et al. 2012), solar cells (Wang et al. 2008), transparent conducting films (Eda et al. 2008; Li et al. 2009) and lithium ion batteries (Wang et al. 2010; Yoo et al. 2008). The 2-D sheet structure of graphene with high surface area provides uniform dispersion of catalysts nanoparticles. In the process of heterogeneous catalysis, the presence of different surface functional groups (e.g., carboxylic, hydroxyl groups) also enhances the surface reactivity as well as adsorption behavior of the catalysts. Many active sites consisted of edges and defects present in the graphitic layer have the ability to modify the electronic property of the catalysts dispersed on it. The modified electronic property can affect the reaction mechanism and ultimately the end product of the reaction (Antolini 2009). In this present work, we have synthesized gold nanoparticles on the reduced graphene oxide support and studied electrochemical reduction of CO_2 by reduced graphene oxide supported gold catalysts. Electrochemical and impedance measurements were carried out to demonstrate the effect of catalyst support and composition on the performance of gold catalyst.

Experimental

Materials

Natural graphite flakes (− 10 mesh, 99.9% metal basis) purchased from Alfa Aesar, hydrazine solution (35 wt%), hydrogen peroxide solution (50 wt% aqueous) was purchased from Merck. $HAuCl_4.3H_2O$ (99.9%) was purchased from Sigma-Aldrich. Unless otherwise stated, reagents were of analytical grade and used as received. Aqueous solutions were prepared with double-distilled deionized (DI) water from Elga Pure Lab System (18.2 MΩ cm).

Synthesis of functionalized graphene oxide

Functionalized graphene oxide (GO) was synthesized from the natural graphite flakes by applying Hummers method (Hummers and Offeman 1958). In a typical synthesis, 1 g of graphite powder was added to 46 mL of conc. H_2SO_4 in an ice bath. Thereafter, $NaNO_3$ (1 g) and $KMnO_4$ (6 g) were added gradually under stirring. The reaction mixture was continually stirred for 1 h at temperature below 0 °C. The mixture was stirred at 35 °C for 1 h and diluted with 100 mL of DI water

and stirred for 1 h. The temperature of the reaction mixture was slowly raised to 95 °C and the reaction was terminated by adding 200 mL DI water and 3 mL 50 wt% H_2O_2 solution. The solid product was separated by centrifugation and washed repeatedly with 3 wt% HCl solution to remove sulfate impurities from the product. The precipitate was dried in an oven at 60 °C for overnight.

Synthesis of gold nanoparticles on reduced graphene oxide

In a typical synthesis of reduced GO (RGO)Au (13.72 wt%), 13 mg of $HAuCl_4.3H_2O$, and 400 μL of oleylamine (OA) were added in 13 mL toluene and the solution was refluxed at 120 °C continued with stirring till the color of the solution changes from yellow to colorless. 52 mg of Graphene Oxide (GO) dissolved in 52-mL DI water was mixed in the above solution. Thirteen milligrams of $NaBH_4$ dissolved in 13-mL methanol was added dropwise to the above mixture with continue stirring at 100 °C temperature and the reaction was stopped after 10 min. The mixture was centrifuged at 10000 rpm three times with ethanol and three times with DI water, respectively. Now, the sample was dried in oven at 60 °C for overnight. The other sample RGOAu (35.51 wt%) was synthesized by identical conditions except the amount of $HAuCl_4.3H_2O$, OA, toluene, and $NaBH_4$ was doubled and amount of GO was 39 mg.

Ink was prepared by adding 2.6 mg of RGOAu in 1-mL DI H_2O and 1-mL isopropyl alcohol (IPA) and 4 μL of Nafion solution.

Electrochemical reduction of CO_2 and analysis of gaseous products formed by gas chromatography

On a polished glassy carbon electrode (GCE) diameter of 1 mm, the prepared RGOAu ink (33 μg/cm^2 catalyst loading) was deposited on it and dried in air. Electrochemical reduction of CO_2 was performed in a three-electrode, two-compartment H-type cell. In one compartment, there were two electrodes: a glassy carbon electrode as a working electrode (WE) and Ag/AgCl electrode as a reference electrode and in another compartment, platinum was used as counter electrodes (CE). All the potentials are converted and expressed with respect to reversible hydrogen electrode (RHE). Both the compartments are filled with 0.5 M $NaHCO_3$ (50 mL) electrolyte and are separated by a Nafion-212 (a proton exchange) membrane. In order to maintain an inert atmosphere, nitrogen gas was purged throughout the electrolyte for 30 min prior to electrochemical measurements, followed by saturation with CO_2 for another 30 min. CO_2 was continuously bubbled throughout the electrolyte during all the durations of electrochemical measurements.

In the gas chromatograph (GC) instrument, first, a standard gaseous mixtures of CO_2, CH_4, CO, etc., was run and their retention times were measured. Then, gaseous sample collected after CO_2 reduction was taken out in an air-tight microsyringe and injected into the GC instrument.

Results and discussion

Microstructural characterizations

Figure 1 shows x-ray diffraction (XRD) patterns of the RGOAu with different weight percent of gold. The phase structure (face-centered cubic, fcc) of the Au NPs was confirmed by XRD. The XRD peaks at 2θ (degrees) 38.15, 44.53, 64.70, 77.60, and 81.84 can be indexed as (111), (200), (220), (311), and (222), planes respectively, which were in agreement with the diffraction pattern of gold (JCPDS 65-2870). The broad peak at 26.52° corresponds to the (002) plane of graphite. The microstructural characterizations of the RGOAu nanocomposites were performed by using both transmission electron microscopy (TEM) and scanning electron microscopy (SEM). Figure 2a, b shows the TEM micrographs of the gold NPs on the reduced graphene oxide. It was observed that the gold NPs were uniformly distributed over the RGO support; the average particle size of Au NPs was approximately 4–5 nm in diameter and spherical in shape. Figure 3 shows the SEM micrographs along with the energy-dispersive x-ray spectroscopy (EDS) of RGOAu. This confirms the observations of the TEM data indicating the well dispersion of gold NPs on the reduced graphene oxide support. The EDS data clearly shows the weight percentage of gold is 13.72% in the RGOAu catalyst. Figure 4a shows the Raman spectra of GO and RGOAu nanocomposite. There are two peaks at 1355 and 1589 cm^{-1}, which correspond to D and G bands of graphene, respectively (Kudin et al. 2008). The G band corresponds to the E_{2g} mode. G band arises from the stretching of the C–C bond in graphitic materials, and is common to all sp^2 carbon systems. D mode is caused by disordered structure of graphene. D band is attributed by in-plane A_{1g}

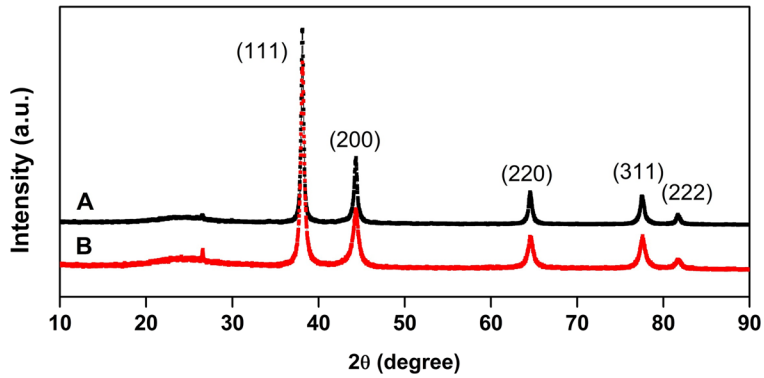

Fig. 1 Powder x-ray diffraction spectra of A, RGOAu (13.72 wt%) and B, RGOAu (35.51 wt%). The XRD peaks at 2θ (degrees) 38.15, 44.53, 64.70, 77.60, and 81.84 corresponds to (111), (200), (220), (311), and (222) planes, respectively, which were in agreement with the diffraction pattern of gold (JCPDS 65-2870). The broad peak at 26.52° corresponds to the (002) plane of graphite

zone-edge mode (Dong et al. 2010b). Compared to GO, the I_D/I_G of RGOAu is higher (0.928 for GO vs. 1.048 for RGOAu), implying that more defects are formed on the RGO sheets which further helps in the enhancement of the electrocatalytic performance. Figure 4b shows the FTIR spectra of RGOAu, bands around 3328 cm^{-1} (OH stretching), 1617 cm^{-1}(C=O stretching), 1475 cm^{-1}(aromatic C=C stretching), 1362 cm^{-1} (C–O carboxy stretching), 1150 cm^{-1} (C–O epoxy stretching), 1058 cm^{-1} (C–O alkoxy stretching) (Marcano et al. 2010), confirming the different oxygen containing functional groups on the graphene sheets. X-ray photoelectron spectroscopy (XPS) analysis of GO and RGOAu has been done to confirm the reduction of GO. Figure 5 shows the XPS spectra of GO and RGOAu. In GO, the prominent peaks for C1s at different binding energies are sp^2 C1s (284.5 eV), sp^3 C1s (285.2 eV), epoxy group (286.3 eV), carboxylic group (287.5 eV) and carbonyl group (289.3 eV). Where as in RGOAu the peaks for C 1 s are sp^2 C1s (284.6 eV), sp^3 C1s (285.4 eV), and carbonyl group (288.3 eV). After reduction with sodium borohydride, the oxygen functionalities of RGO were reduced in larger extent and from Fig. 5b, it is clearly evident that the peak corresponding to the sp^2 carbon at 284.5 eV was the major feature of the C1s region in case of RGOAu. On the same way, the intensity of the sp3 carbon peak at 285.2 eV was considerably reduced. This clearly reflects the repair of GO in RGOAu during synthesis process. In order to demonstrate that gold nanoparticles have formed on the RGO sheets, the RGOAu was subjected to UV-VIS spectroscopic analysis. Figure S1 shows the UV-VIS spectra of RGOAu. The absorption peak at ~260 nm is of graphene sheet (Li et al. 2008). The plasmon

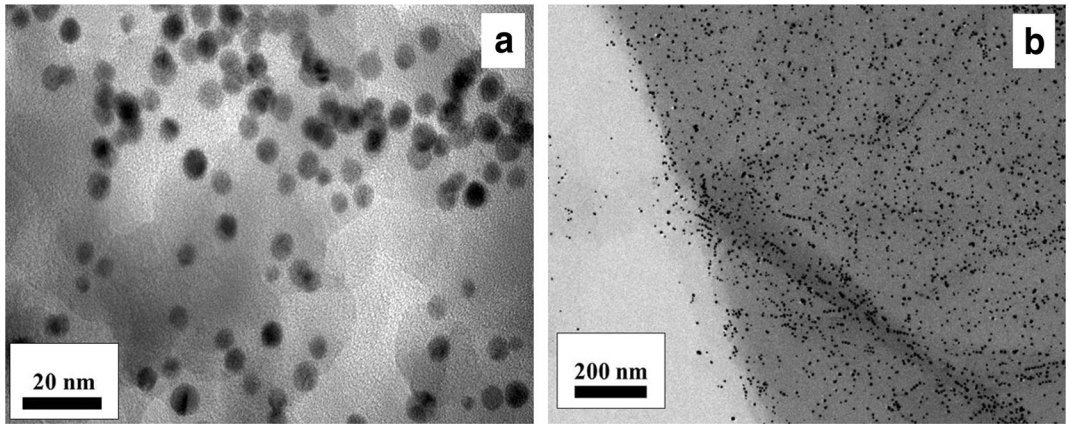

Fig. 2 Transmission electron microscopy (TEM) micrographs of RGOAu. **a** High-magnification TEM micrograph of RGOAu. **b** Low-magnification TEM micrograph of RGOAu. It was observed that the gold NPs were uniformly distributed over the reduced graphene oxide (RGO) support and the average particle size of Au NPs was approximately 4–5 nm in diameter and spherical in shape

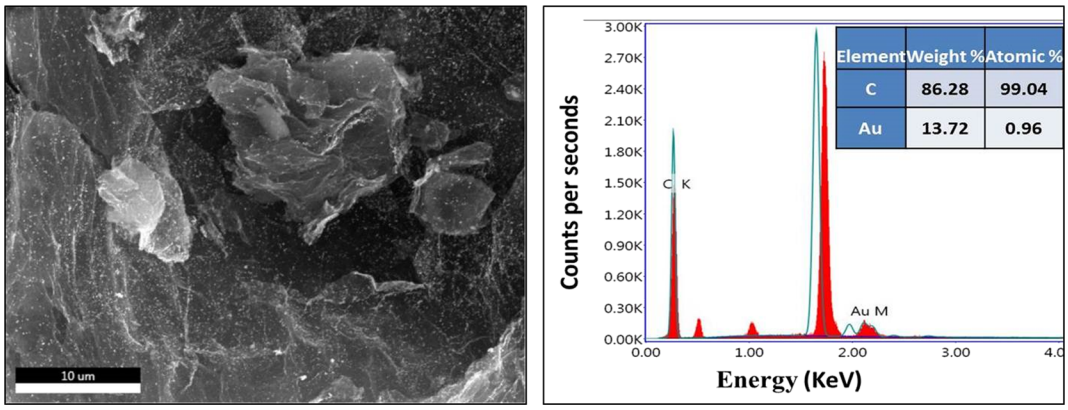

Fig. 3 Scanning electron microscopy (SEM) micrograph and energy-dispersive x-ray spectroscopy (EDS) data of RGOAu. The EDS data clearly shows 13.72 weight percentage of gold in RGOAu catalyst

absorption of gold nanoparticles in the RGOAu appears at ~ 540 nm in the UV-Vis spectrum (Haiss et al. 2007).

Electrochemical measurements of CO_2 reduction on RGOAu/GCE

Electrochemical measurements were performed on an AUT86543 Metrohm Autolab B. V. electrochemical workstation. Figure 6a shows cyclic voltammetry (CV) measurements of RGOAu (13.72 wt%) in 0.5 M $NaHCO_3$ electrolyte solution in the range of − 1.75 to 1.75 V vs. RHE at a scan rate of 20 mV/s. In the presence of CO_2, onset potential has been shifted to more negative potential than in presence of nitrogen and the change in onset potential was found to be 230 mV. This negative shift of onset potential was due to adsorbed species associated on the catalyst surface and reduction of carbon dioxide on the surface initiates (Tang et al. 2012; Xu et al. 2012). In aqueous medium, CO_2 reduction and hydrogen evolution reaction (HER) are quite competitive against each other. For that reason, we have chosen the potential for chronoamperometry far beyond the HER potential. Figure 6b shows the chronoamperometry data of carbon dioxide reduction at three different potentials: 0.35, − 0.24, and − 0.44 V

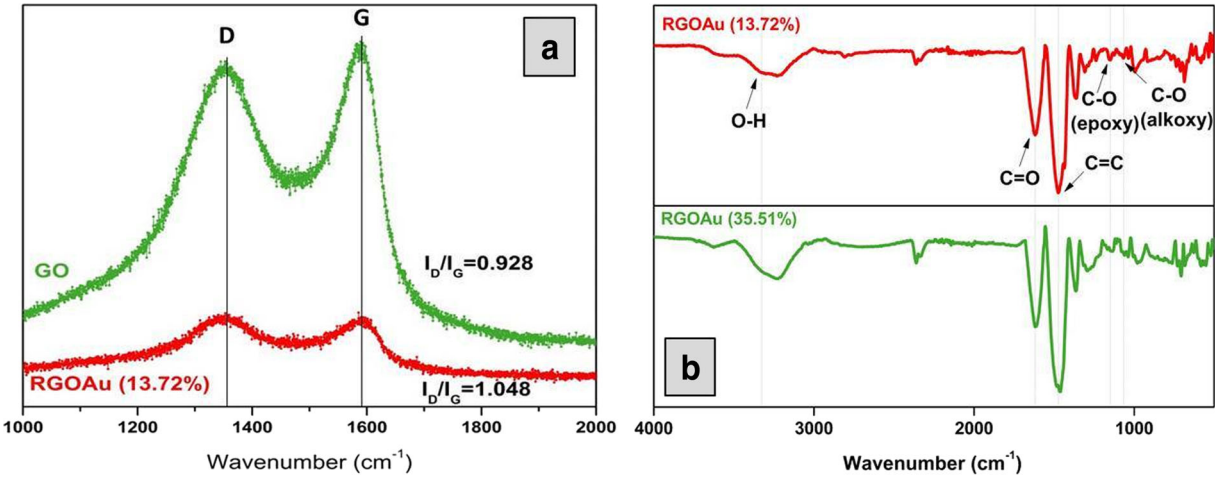

Fig. 4 **a** Raman spectra of GO and RGOAu. The two peaks at 1355 and 1589 cm^{-1} correspond to D and G bands of graphene, respectively. G band arises from the stretching of the C–C bond in graphitic materials and is common to all sp^2 carbon systems. The D mode is caused by disordered structure of graphene. Compared to GO, the I_D/I_G of RGOAu is higher (0.928 for GO vs. 1.048 for RGOAu), implying that more defects are formed on the RGO sheets which further helps in the enhancement of the electrocatalytic performance. **b** FTIR spectra of RGOAu. The bands at 3328 cm^{-1} (OH stretching), 1617 cm^{-1} (C=O stretching), 1475 cm^{-1} (aromatic C=C stretching), 1362 cm^{-1} (C–O carboxy stretching), 1150 cm^{-1} (C–O epoxy stretching), and 1058 cm^{-1} (C–O alkoxy stretching) confirmed the presence of different oxygen containing functional groups on the graphene sheets

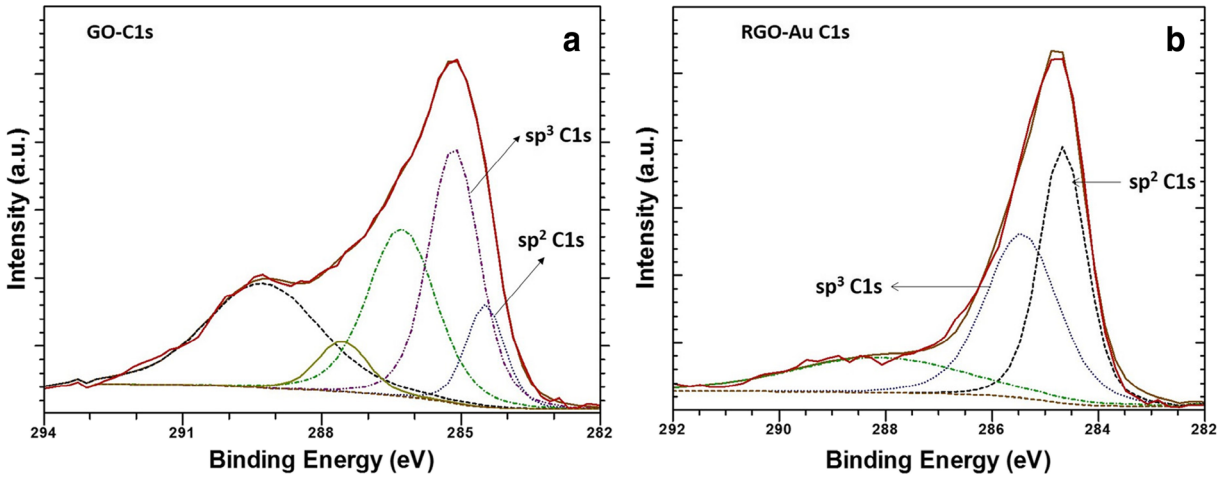

Fig. 5 X-ray photoelectron spectroscopy (XPS) spectra of **a** GO and **b** RGOAu to confirm the reduction of GO. The peaks in GO for C1s at different binding energies are sp^2 C1s (284.5 eV), sp^3 C1s (285.2 eV), epoxy group (286.3 eV), carboxylic group (287.5 eV), and carbonyl group (289.3 eV). While in case of RGOAu, the peaks for C1s are sp^2 C1s (284.6 eV), sp^3 C1s (285.4 eV) and carbonyl group (288.3 eV)

(all vs. RHE), respectively, for RGOAu (13.72 wt%). From the chronoamperometry data, it is clearly visible that at 0.35 V, the current obtained is very low indicating a poor reduction of carbon dioxide at this potential. At − 0.24 V, the reduction of CO_2 is appreciable (around 20 μA/cm^2). Since the theoretical equilibrium potential for CO_2/CO is − 0.11 V vs. RHE, thus, − 0.24 V corresponds to 0.13 V of overpotential for CO production (η_{CO}). Current for CO_2 reduction increases to ca. three times when more negative potential (− 0.44 V) was applied over 1 h of electrolysis. During chronoamperometry experiments, the gaseous products were injected out at the regular intervals and monitored the products of the reaction by GC. We have observed the selective formation of CO in the cathode. No other gaseous product had been detected in the cathodic compartment of H cell.

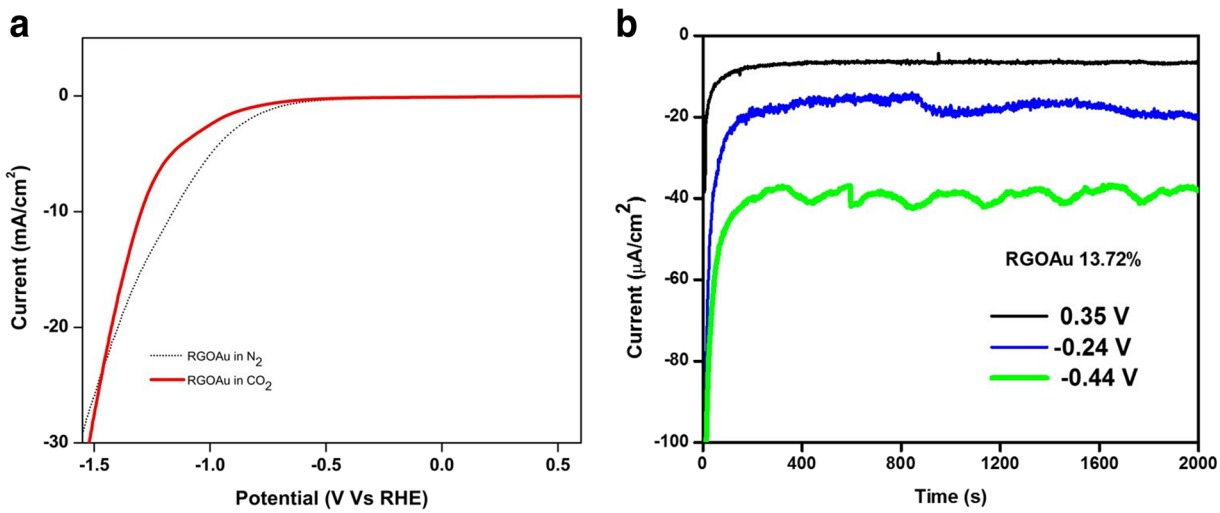

Fig. 6 **a** Cyclic voltammetry (CV) curves of RGOAu (13.72 wt%) in N_2 and CO_2 saturated in 0.5 M $NaHCO_3$ electrolyte solution in the range of − 1.75 to 1.75 V vs. RHE at a scan rate of 20 mV/s. In the presence of CO_2, onset potential has been shifted to more negative potential than in presence of nitrogen and the change in onset potential was found to be 230 mV. **b** Chronoamperometry of RGOAu (13.72 wt%) at 0.35, − 0.24, and −0 .44 V potentials, respectively. At 0.35 V, the current density obtained is very low but at − 0.24 V, current density is around 20 μA/cm^2. Further, at more negative potential (− 0.44 V), current density for CO_2 reduction increases to ca. three times

To observe the effect of concentration of gold on the conversion of carbon dioxide into CO, another composition of gold was prepared, labeled as RGOAu (35.51 wt%). Similar CO_2 reduction experiments were performed with RGOAu (35.51 wt%). As revealed by CVs in Fig. 7a, RGOAu (35.51 wt%) exhibited higher catalytic activity than RGOAu (13.72 wt%). For instance, RGOAu (35.51 wt%) displayed a current density of 50.95 mA/cm^2 at − 1.50 V vs. RHE, which was ca. 1.65 times larger than that of RGOAu (13.72 wt%). From Fig. 7a, it is clearly evident that the onset potential for CO_2 reduction is shifted towards positive potential of 240 mV indicating RGOAu (35.51 wt%) is catalytically more active for carbon dioxide reduction than RGOAu (13.72 wt%). Figure 7b indicates the presence of more active catalytic sites in RGOAu (35.51 wt%) which has higher reaction rate for carbon dioxide reduction than RGOAu (13.72 wt%) (Whipple and Kenis 2010). To observe the effect of degree of reduction of graphene oxide on the catalytic activity of RGOAu, we have prepared a new set of sample where the amount of reducing agent ($NaBH_4$) has been used twice than before. It has been previously reported (Shin et al. 2009) that $NaBH_4$ reduction decreases the sheet resistance of graphene oxide and enhances the conductivity of graphene oxide by removing some of the carbonyl and hydroxyl functional groups of graphene oxide. Hence, for the same amount of gold, the more reduced GO gives better onset potential as well as higher current density for CO_2 reduction. It is clear from Fig. 8 that RGOAu synthesized with double the weight of $NABH_4$ is showing better CO_2 reduction activity. So, higher degree of reduction of graphene oxide increases the CO_2 reduction catalytic activity of RGOAu. We have synthesized different weight percentages of Au which are 38.76, 48.56, and 76.69%. From Fig. 9, it is clearly evident that the activity of pure Au NPs is poorer than RGOAu (38.76 wt%). Further, the onset potential for CO_2 reduction decreases from 38.76 to 48.56% but when Au wt% is increased to 76.69%, there is almost no change in onset potential as compared with 48.56%. In addition to this, the current density at − 0.98 V vs. RHE of 76.69% is 2.5 times lower than that of 48.56%. So, the optimum concentration of Au in RGOAu is found to be 48.56%, i.e., RGOAu (48.56 wt%) for the catalytic reduction of CO_2. This finding was further confirmed by the electrochemical impedance spectroscopy measurements which investigated the role of impedance on the performance of the catalyst. The electrochemical impedance spectroscopy (EIS) analysis was carried out at a potential of − 1.0 V vs. RHE from 100 KHz to 0.1 Hz frequency. Figure 10a shows the Nyquist plots and the equivalent circuit for the electrochemical cells. The charge transfer resistance (R_p) values of the electrochemical cells were obtained from the diameters of the semicircle. The impedance (R_p) value for RGOAu (35.51 wt%) and RGOAu (13.72 wt%) was found to be 257 and 754 Ω, respectively.

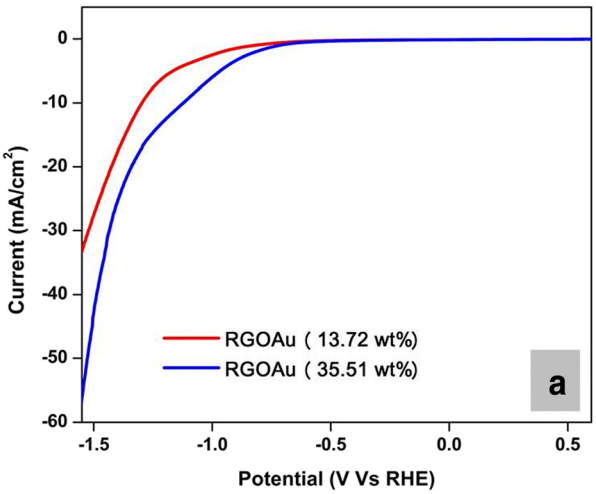

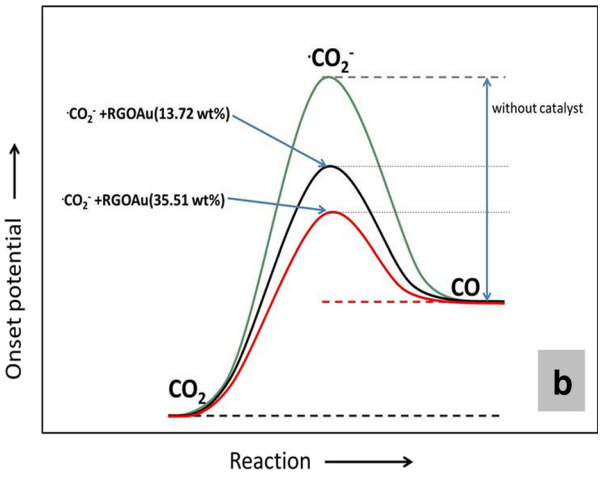

Fig. 7 **a** CVs of RGOAu catalysts in CO_2 saturated in 0.5 M $NaHCO_3$ aqueous solution. For RGOAu (35.51 wt%), the onset potential for CO_2 reduction is shifted towards positive potential of 240 mV indicating that it is catalytically more active than RGOAu (13.72 wt%). **b** Schematic of CO_2 reduction with two different RGOAu catalysts. It indicates more active catalytic sites are present in RGOAu (35.51 wt%), which has higher reaction rate for carbon dioxide reduction than RGOAu (13.72 wt%)

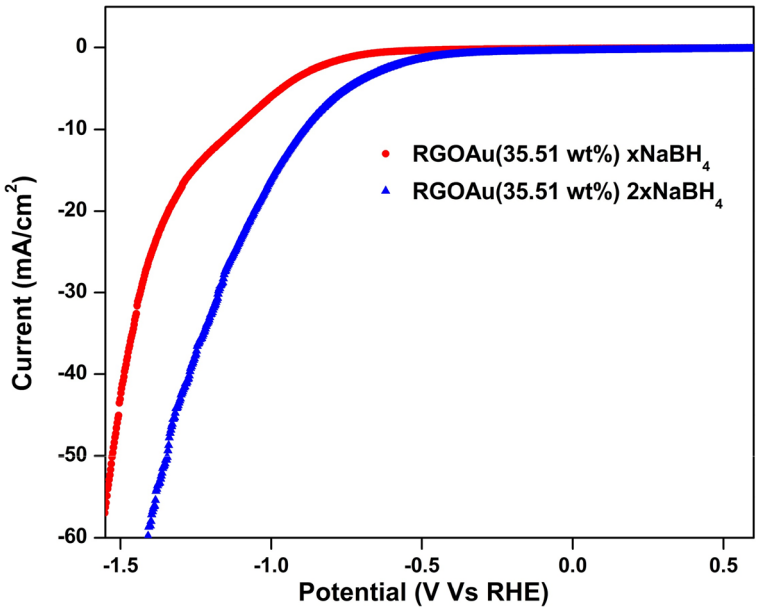

Fig. 8 CVs of RGOAu (35.51 wt%) with different amounts of reducing agent ($NaBH_4$) used in CO_2 saturated in 0.5 M $NaHCO_3$ aqueous solution

Transfer of electron from CO_2 to CO_2^- (Eq. 1) is generally regarded as the rate-determining step for CO_2 reduction (Hori et al. 1986; Liu et al. 2010; Chen et al. 2012; Yan et al. 2012).

$$CO_2 + e^- \rightarrow CO_2^- \quad (1)$$

$$CO_2^- + 2H^+ + e^- \rightarrow CO + H_2O \quad (2)$$

CO_2 is a linear molecule whereas CO_2^- is a bent species and the bent radical anion as well as it is highly unstable species and the stabilization of this intermediate is the major concern for CO_2 reduction (Dong et al. 2010b). The smaller R_p value suggested that RGOAu (35.51 wt%) ensures the fast electron transfer from the catalyst to the adsorbed CO_2 forming the CO_2^- radical anion intermediate. In addition to obtain further understandings, their Tafel plots were investigated (Fig. 10b).

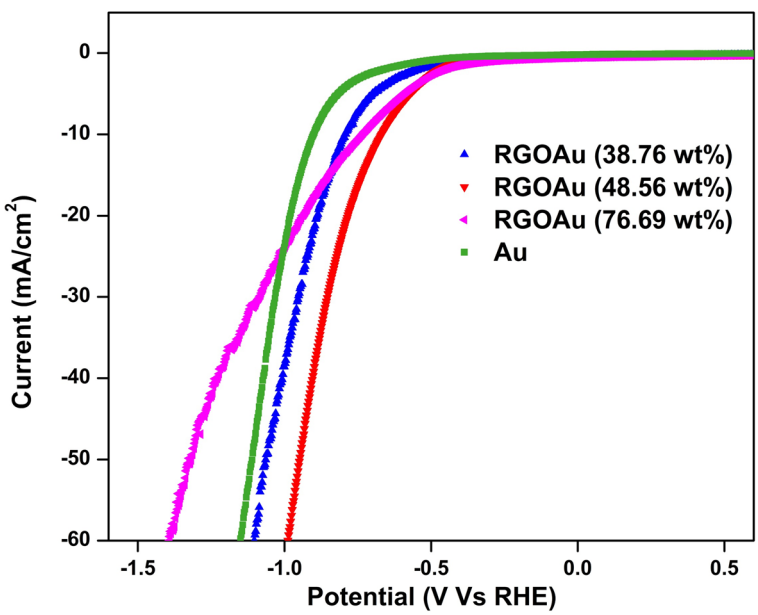

Fig. 9 CVs of Au NPs and RGOAu with different percentage in CO_2 saturated in 0.5 M $NaHCO_3$ aqueous solution

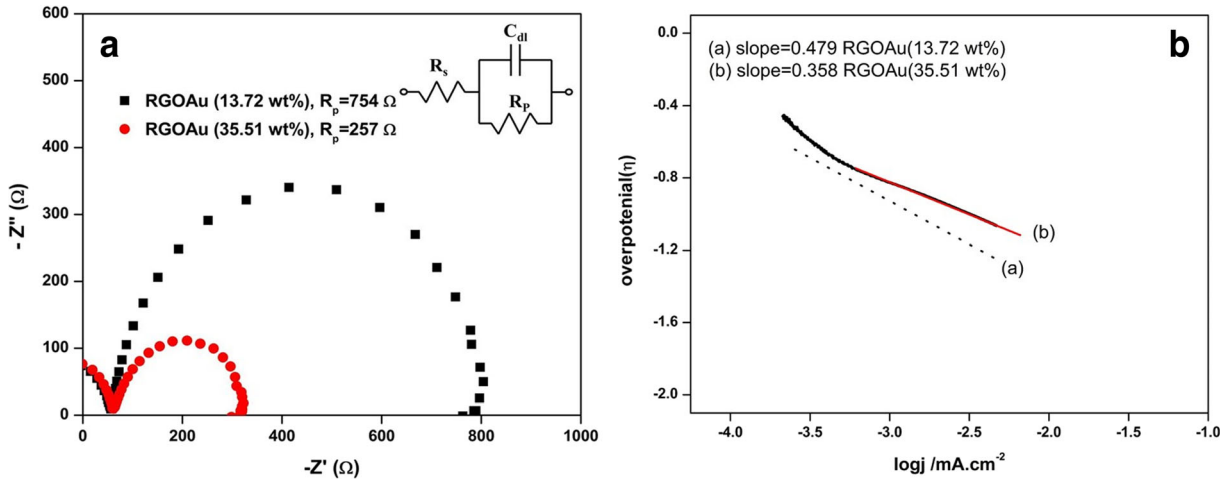

Fig. 10 **a** Nyquist plots and their equivalent circuit for the electrochemical cells of the two RGOAu catalysts. R_s = ohmic serial resistance, R_p = charge transfer resistance, and C_{dll} = double-layer capacitance. **b** Tafel plots for producing CO. Tafel slope of RGOAu (35.51 wt%) was 0.358 and that of RGOAu (13.72 wt%) was 0.479, indicating that RGOAu (13.72 wt%) electrode exhibited much slower kinetics than the RGOAu (35.51 wt%)

The resulting Tafel slope of RGOAu (35.51 wt%) was 0.358 and that of RGOAu (13.72 wt%) was 0.479, indicating that RGOAu (13.72 wt%) electrode exhibited much slower kinetics than the RGOAu (35.51 wt%). So, it proved that RGOAu (35.51 wt%) was able to stabilize the CO_2^- intermediate much better than RGOAu (13.72 wt%) and led to much faster CO_2 reduction rate. The pioneer work of Hori et al. (1985) showed the selectivity and faradaic efficiencies for the electrochemical reduction of carbon dioxide to carbon monoxide was different for different metals. Among all the different metals, it was observed that gold showed the highest faradaic efficiency for converting carbon dioxide into carbon monoxide. Molecular orbital studies indicated that in case of CO_2, the coordination bond is stabilized by the back donation from the filled d orbitals of metal atom to empty antibonding orbital of carbon dioxide (Hori et al. 1986). There are three modes of coordination existing between the metal–CO_2 bonding and it is C coordination which is favored in case of gold electrode (Hori et al. 1994). The CO_2 reduction property of metal largely depends upon the strength of back

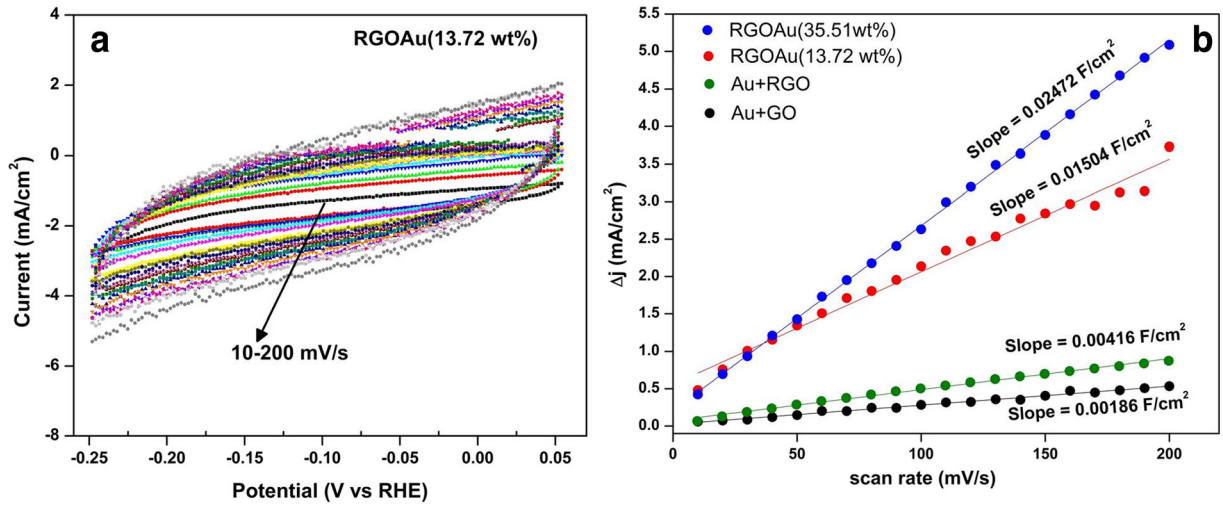

Fig. 11 **a** CVs of RGOAu (13.72 wt%) with different scan rates from 10 to 200 mV s^{-1}. **b** The capacitive current at − 0.10 V as a function of scan rate for RGOAu (35.51 wt%), RGOAu (13.72 wt%), 5.5 nm Au NPs physically mixed with reduced graphene oxide (RGO) and with graphene oxide (GO)

bonding between metal to ligand. The adsorbed formate radical anion (CO_2^-) greatly stabilized by the strong charge transfer from gold to ligand. Thus, increment in the amount of gold in the second catalyst enhances the activity of catalyst due to availability of more active sites.

Support material RGO also plays an important role in improving the activity of the catalysts. The density functional study carried by Hansen et al. (2013) indicated that although the activation of CO_2 through COOH formation on Au surface required high increase in free energy (at the reversible potential), on the contrary, the standard free energy of desorption of CO was close to zero. Thus, facile removal of CO from Au surfaces was highly favorable. This was quite contradictory in case of other metals like Pd, Ni, and Pt. Au has a great advantage over others due to its stronger binding of COOH on the surface with a weaker binding of CO, eventually improving the turnover rate (TOR) for the electrochemical reduction of carbon dioxide and evolution of CO. Now, RGO-supported Au has an additional advantage for this purpose.

First principle study (DFT) done by Lim D.H. et al. (Lim et al. 2014) showed that the electronic and structural properties of copper can be modified by using defective graphene-supported Cu nanoparticles which enhances the electrochemical reduction of CO_2 to various hydrocarbon fuels. The DFT study showed that in Cu-defective graphene system, the uncoordinated sites significantly lower the energy barriers of the system, and thus, it increased the energy efficiency of the CO_2 reduction. In our present work, Raman and FTIR spectroscopy confirm the presence of defects on the support material RGO. We have used electrochemical double-layer capacitance (EDLC, C_{dll}) method to investigate electrochemical active surface area (Lei et al. 2016). To investigate the electrochemical double-layer capacitance (C_{dll}), cyclic voltammetry was performed in the region from 0.05 to −0.25 V at rates varying from 10 to 200 mV s^{-1} (Fig. 11a). To understand the effect of defects of RGO on the activity of gold, we have prepared similar size of gold nanoparticles and physically mixed it with GO and RGO. The measured electrochemical double layer capacitance (C_{dll}) of RGOAu (35.51 wt%) and RGOAu (13.72 wt%) were found to be 24.7 and 15 mF/cm^2, respectively. Whereas C_{dll} value of 5.5 nm Au nanoparticles physically mixed with graphene oxide (Au + GO) and reduced graphene oxide

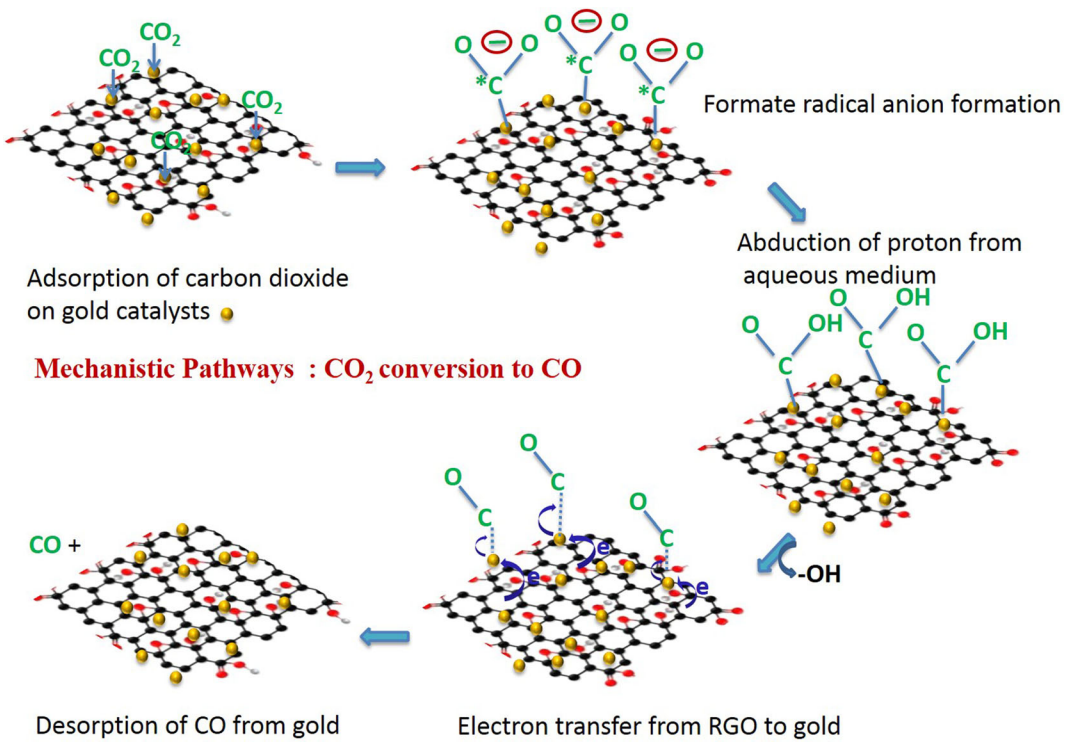

Fig. 12 Schematic of the mechanistic path of carbon dioxide reduction on RGO-supported Au

(Au + RGO) were 1.86 and 4.16 mF/cm^2, respectively (Fig. 11b). It is clear that C_{dll} values for RGOAu are much higher than Au NPs physically mixed with GO and RGO. Similar kind of experimental observation was performed by other group on metallic tin quantum sheets confined in graphene shows high-efficiency carbon dioxide electroreduction (Lei et al. 2016). Investigating through the experimental data, a mechanism for CO_2 reduction has been proposed (Fig. 12). The formation of formate radical anion was stabilized by high electron density present on the oxygen atoms due to back donation from gold. This leads to higher abduction of proton in the aqueous medium and ultimate formation of CO by removal of hydroxyl anions. The defect sites on RGO were enabling the facile desorption of CO from Au surfaces by electron transfer from RGO to Au. This is a clear demonstration that how the interaction of the support materials with the adsorbates and the promotional effect of support to electron transport leads to the enhanced activity of the RGO-supported gold catalysts.

Conclusion

In this work, we have successfully synthesized Au NPs with different weight percent on defective reduced graphene oxide support. RGOAu catalysts show significant activity towards the selective reduction of carbon dioxide to carbon monoxide by electrochemical method. The lower overpotential of carbon dioxide reduction can be attributed due to the presence of support material where the defect sites play a significant role for reducing the overpotential for carbon dioxide reduction. In addition, the rate of carbon dioxide reduction was also found to be greatly affected by the concentration of Au on the composites in which higher gold concentration shows lower impedance and Tafel slope with low overpotential for carbon dioxide reduction. The investigated aspects are relevant for understanding the role of modified support materials on the selective reduction of carbon dioxide into other commercially valuable fuels.

Acknowledgements We acknowledge the Human Resource development (HRD) for financial support and Advanced Material Research Centre (AMRC), IIT Mandi, for providing experimental facilities. AH thanks IIT Mandi for its seed grant and the Department of Science and Technology (DST), India, for providing financial support under Young Scientist Project Scheme.

Funding information This work was supported by Science and Engineering Research Board (SERB) with the grant no: YSS/2014/000997 under Young Scientist Scheme.

Compliance with ethical standard

Conflict of interest The authors declare that they have no competing interests.

References

Antolini E (2009) Carbon supports for low-temperature fuel cell catalysts. Appl Catal B Environ 88(1–2):1–24. https://doi.org/10.1016/j.apcatb.2008.09.030

Benson EE, Kubiak CP, Sathrum AJ, Smieja JM (2009) Electrocatalytic and homogeneous approaches to conversion of CO2 to liquid fuels. Chem Soc Rev 38(1):89–99. https://doi.org/10.1039/B804323J

Bradford M, Vannice M (1999) CO2 reforming of CH4. Catal Rev 41(1):1–42. https://doi.org/10.1081/CR-100101948

Chen Y, Li CW, Kanan MW (2012) Aqueous CO2 reduction at very low overpotential on oxide-derived Au nanoparticles. J Am Chem Soc 134(49):19969–19972. https://doi.org/10.1021/ja309317u

Dong L, Gari RRS, Li Z, Craig MM, Hou S (2010a) Graphene-supported platinum and platinum–ruthenium nanoparticles with high electrocatalytic activity for methanol and ethanol oxidation. Carbon 48(3):781–787. https://doi.org/10.1016/j.carbon.2009.10.027

Dong X, Huang W, Chen P (2010b) In situ synthesis of reduced graphene oxide and gold nanocomposites for nanoelectronics and biosensing. Nanoscale Res Lett 6(1):60

Eda G, Fanchini G, Chhowalla M (2008) Large-area ultrathin films of reduced graphene oxide as a transparent and flexible electronic material. Nat Nanotechnol 3(5):270–274. https://doi.org/10.1038/nnano.2008.83

Gao S, Lin Y, Jiao X, Sun Y, Luo Q, Zhang W, Li D, Yang J, Xie Y (2016) Partially oxidized atomic cobalt layers for carbon dioxide electroreduction to liquid fuel. Nature 529(7584):68–71. https://doi.org/10.1038/nature16455

Geim AK, Novoselov KS (2007) The rise of graphene. Nat Mater 6(3):183–191. https://doi.org/10.1038/nmat1849

Haiss W, Thanh NTK, Aveyard J, Fernig DG (2007) Determination of size and concentration of gold nanoparticles from UV−Vis spectra. Anal Chem 79(11):4215–4221. https://doi.org/10.1021/ac0702084

Hansen HA, Varley JB, Peterson AA, Nørskov JK (2013) Understanding trends in the electrocatalytic activity of metals and enzymes for CO2 reduction to CO. J Phys Chem Lett 4(3):388–392. https://doi.org/10.1021/jz3021155

Hori Y (2008) Electrochemical CO2 reduction on metal electrodes. In: Vayenas CG, White RE, Gamboa-Aldeco ME (eds) Modern aspects of electrochemistry. Springer, New York, p 89–189. https://doi.org/10.1007/978-0-387-49489-0_3

Hori Y, Kikuchi K, Suzuki S (1985) Production of CO and CH4 in electrochemical reduction of CO2 at metal electrodes in

aqueous hydrogencarbonate solution. Chem Lett 14(11): 1695–1698. https://doi.org/10.1246/cl.1985.1695

Hori Y et al (1986) Production of methane and ethylene in electrochemical reduction of carbon dioxide at copper electrode in aqueous hydrogencarbonate solution. Chem Lett 15(6): 897–898

Hori Y, Murata A, Kikuchi K, Suzuki S (1987) Electrochemical reduction of carbon dioxides to carbon monoxide at a gold electrode in aqueous potassium hydrogen carbonate. J Chem Soc Chem Commun (10):728–729. https://doi.org/10.1039/c39870000728

Hori Y, Murata A, Takahashi R (1989) Formation of hydrocarbons in the electrochemical reduction of carbon dioxide at a copper electrode in aqueous solution. J Chem Soc Faraday Trans 1 85(8):2309–2326

Hori Y, Wakebe H, Tsukamoto T, Koga O (1994) Electrocatalytic process of CO selectivity in electrochemical reduction of CO2 at metal electrodes in aqueous media. Electrochim Acta 39(11):1833–1839. https://doi.org/10.1016/0013-4686(94)85172-7

Hummers WS, Offeman RE (1958) Preparation of graphitic oxide. J Am Chem Soc 80(6):1339–1339. https://doi.org/10.1021/ja01539a017

Jitaru M (2007) Electrochemical carbon dioxide reduction-fundamental and applied topics. J Univ Chem Technol Metall 42(4):333–344

Kapusta S, Hackerman N (1983) The electroreduction of carbon dioxide and formic acid on tin and indium electrodes. J Electrochem Soc 130(3):607–613. https://doi.org/10.1149/1.2119761

Köleli et al (2003) Electrochemical reduction of CO_2 at Pb- and Sn-electrodes in a fixed-bed reactor in aqueous K_2CO_3 and $KHCO_3$ media. J Appl Electrochem 33:447–450. https://doi.org/10.1023/A:1024471513136

Kudin KN, Ozbas B, Schniepp HC, Prud'homme RK, Aksay IA, Car R (2008) Raman spectra of graphite oxide and functionalized graphene sheets. Nano Lett 8(1):36–41. https://doi.org/10.1021/nl071822y

Lei F, Liu W, Sun Y, Xu J, Liu K, Liang L, Yao T, Pan B, Wei S, Xie Y (2016) Metallic tin quantum sheets confined in graphene toward high-efficiency carbon dioxide electroreduction. Nat Commun 7:12697. https://doi.org/10.1038/ncomms12697

Li D, Muller MB, Gilje S, Kaner RB, Wallace GG (2008) Processable aqueous dispersions of graphene nanosheets. Nat Nano 3(2):101–105. https://doi.org/10.1038/nnano.2007.451

Li Y, Tang L, Li J (2009) Preparation and electrochemical performance for methanol oxidation of pt/graphene nanocomposites. Electrochem Commun 11(4):846–849

Lim D-H, Jo JH, Shin DY, Wilcox J, Ham HC, Nam SW (2014) Carbon dioxide conversion into hydrocarbon fuels on defective graphene-supported Cu nanoparticles from first principles. Nano 6(10):5087–5092

Liu C, Yu Z, Neff D, Zhamu A, Jang BZ (2010) Graphene-based supercapacitor with an ultrahigh energy density. Nano Lett 10(12):4863–4868. https://doi.org/10.1021/nl102661q

Marcano DC, Kosynkin DV, Berlin JM, Sinitskii A, Sun Z, Slesarev A, Alemany LB, Lu W, Tour JM (2010) Improved synthesis of graphene oxide. ACS Nano 4(8):4806–4814. https://doi.org/10.1021/nn1006368

Middleton RS, Eccles JK (2013) The complex future of CO2 capture and storage: variable electricity generation and fossil fuel power. Appl Energy 108:66–73. https://doi.org/10.1016/j.apenergy.2013.02.065

Nie X, Esopi MR, Janik MJ, Asthagiri A (2013) Selectivity of CO2 reduction on copper electrodes: the role of the kinetics of elementary steps. Angew Chem Int Ed 52(9):2459–2462. https://doi.org/10.1002/anie.201208320

Park S, Ruoff RS (2009) Chemical methods for the production of graphenes. Nat Nanotechnol 4(4):217–224. https://doi.org/10.1038/nnano.2009.58

Shin HJ, Kim KK, Benayad A, Yoon SM, Park HK, Jung IS, Jin MH, Jeong HK, Kim JM, Choi JY (2009) Efficient reduction of graphite oxide by sodium borohydride and its effect on electrical conductance. Adv Funct Mater 19(12):1987–1992. https://doi.org/10.1002/adfm.200900167

Stankovich S, Dikin DA, Dommett GH, Kohlhaas KM, Zimney EJ, Stach EA, Piner RD, Nguyen ST, Ruoff RS (2006) Graphene-based composite materials. Nature 442(7100): 282–286. https://doi.org/10.1038/nature04969

Tang W, Peterson AA, Varela AS, Jovanov ZP, Bech L, Durand WJ, Dahl S, Nørskov JK, Chorkendorff I (2012) The importance of surface morphology in controlling the selectivity of polycrystalline copper for CO2 electroreduction. Phys Chem Chem Phys 14(1):76–81. https://doi.org/10.1039/C1CP22700A

Wang X, Zhi L, Müllen K (2008) Transparent, conductive graphene electrodes for dye-sensitized solar cells. Nano Lett 8(1):323–327. https://doi.org/10.1021/nl072838r

Wang H, Cui L-F, Yang Y, Sanchez Casalongue H, Robinson JT, Liang Y, Cui Y, Dai H (2010) Mn3O4—graphene hybrid as a high-capacity anode material for lithium ion batteries. J Am Chem Soc 132(40):13978–13980. https://doi.org/10.1021/ja105296a

Whipple DT, Kenis PJ (2010) Prospects of CO2 utilization via direct heterogeneous electrochemical reduction. J Phys Chem Lett 1(24):3451–3458. https://doi.org/10.1021/jz1012627

Xu Z, Lai E, Shao-Horn Y, Hamad-Schifferli K (2012) Compositional dependence of the stability of AuCu alloy nanoparticles. Chem Commun 48(45):5626–5628. https://doi.org/10.1039/c2cc31576a

Yan J, Fan Z, Sun W, Ning G, Wei T, Zhang Q, Zhang R, Zhi L, Wei F (2012) Advanced asymmetric supercapacitors based on Ni(OH)2/graphene and porous graphene electrodes with high energy density. Adv Funct Mater 22(12):2632–2641. https://doi.org/10.1002/adfm.201102839

Yoo E, Kim J, Hosono E, Zhou H-S, Kudo T, Honma I (2008) Large reversible Li storage of graphene nanosheet families for use in rechargeable lithium ion batteries. Nano Lett 8(8): 2277–2282. https://doi.org/10.1021/nl800957b

Zhu W, Michalsky R, Metin Ö, Lv H, Guo S, Wright CJ, Sun X, Peterson AA, Sun S (2013) Monodisperse Au nanoparticles for selective electrocatalytic reduction of CO2 to CO. J Am Chem Soc 135(45):16833–16836. https://doi.org/10.1021/ja409445p